E-9346

HTD-Vol. 284/AMD-Vol. 182, Transport Phenomena in Solidification
ASME 1994

NUMERICAL AND EXPERIMENTAL STUDY OF TRANSPORT PHENOMENA IN DIRECTIONAL SOLIDIFICATION OF SUCCINONITRILE

Henry C. de Groh III
NASA Lewis Research Center
Cleveland, Ohio

Minwu Yao
Ohio Aerospace Institute
Brook Park, Ohio

ABSTRACT

A numerical and experimental study of the growth of succinonitrile (SCN) using a horizontal Bridgman furnace and transparent glass ampoule was conducted. Two experiments were considered: one in which the temperature profile was fixed relative to the ampoule (no-growth case); and a second in which the thermal profile was translated at a constant rate (steady growth case). Measured temperature profiles on the outer surface of the ampoule were used as thermal boundary conditions for the modelling. The apparent heat capacity formulation combined with the variable viscosity method was used to model the phase change in SCN. Both 2-D and 3-D models were studied and numerical solutions obtained using the commercial finite element code, FIDAP[1]. Comparison of the numerical results to experimental data showed excellent agreement. The complex 3-D shallow-cavity flow in the melt, differences between 2-D and 3-D models, effects of natural convection on the thermal gradient and shape of the solid/liquid interface, and the sensitivity of simulations to specific assumptions, are also discussed.

1. NASA does not endorse commercial products. Details about the products named in this paper were included for completeness and accuracy. No endorsement or criticism of these products by NASA should be assumed.

INTRODUCTION

The manufacture of electronic materials and optoelectronic devices demands high-quality crystals. It is known (Brown, 1988) that the quality of crystals grown from the melt is strongly influenced by the interaction between heat and mass transport and fluid flow during the solidification process. Consequently, vigorous experimental and numerical research activities have been conducted in recent years in order to enhance the understanding of transport phenomena and fluid motion during crystal growth (Sparrow, et al., 1979, Chang and Brown, 1984, Pimputkar and Ostrach, 1981, Langlois, 1984, Glicksman et al., 1986, Yeoh et al., 1990).

Horizontal Bridgman growth is a widely used technique in crystal growth research. During horizontal Bridgman growth under terrestrial conditions (1-g), the so-called "shallow-cavity" convective flow can be quite strong (Arnold et al., 1991, Chait, 1990). Generally, shallow-cavity flow is complex, three-dimensional in nature, and about two orders of magnitude stronger than convection during vertical Bridgman growth. Previous studies show that this gravity-driven convective flow can have a significant impact on growth rate, solid/liquid (s/l) interface shape and segregation of impurities (Brown, 1988, Sparrow, et al., 1979, Chang and Brown, 1984, Pimputkar and Ostrach, 1981, Langlois, 1984, Glicksman et al., 1986, Yeoh et al., 1990).

Among the materials used for understanding solidification and crystal growth behavior, a transparent plastic material called succinonitrile (SCN) has been gaining increasing interest from experimentalists (Mennetrier et al., 1991, Chopra and Glicksman, 1988, Inotomi et al., 1993). The main advantages of SCN for laboratory study of crystal growth are as follows. First, SCN is widely used as an analog to metals. For example, a SCN-acetone alloy can be used as a model material for metallic solidification study. Second, because of its transparency, the fluid motion can be simultaneously observed through a transparent ampoule. Thus some other important physical characteristics, such as the growth rate, interface shape, strength of convective flow and even the concentration profile, can be quantitatively determined using op-

tical devices. Third, it has a conveniently low melting point ($T_m = 58.24°C$) and grows non-faceted. Finally, its physical and chemical properties have been well established (Chopra et al., 1988).

In previous publications (Mennetrier, 1991, Yeoh et al., 1992, Yao and de Groh, 1993), the authors and their co-workers have reported the effects of natural convection on interface shape during horizontal Bridgman growth of SCN. Fairly good agreement was achieved among experiments and two numerical simulations, one based on the finite element method (FEM) and a second used the finite difference method (FDM). However, those works were restricted to study of the no-growth case. In addition, the study of interface shape was limited to a mid-center vertical plane (symmetry plane), and no direct temperature measurements were available from inside the ampoule.

In the present work, we consider two new experiments (de Groh and Lindstrom, 1994). They are a refined no-growth experiment with temperature being measured inside the SCN sample and a steady growth solidification experiment with non-zero growth rate. In the steady growth case experimental conditions were measured after steady state was achieved. However, the numerical simulation also models the transient between zero and steady growth. For the two experiments, the interface shape was measured not only at the mid-center vertical plane but also at other two-dimensional planes, which together provide a three-dimensional picture of the s/l interface. Measured temperature profiles on the outer surface of the ampoule are imposed as thermal boundary conditions for the FEM modelling.

The primary objectives of this work are as follows: to determine quantitatively how conduction and convection influence interface shape, to evaluate the numerical model and computer code through comparison with experiments, to address some relevant issues in the numerical modelling, such as the difference between 2-D and 3-D models, and to provide benchmark numerical and experimental data for researchers in this field.

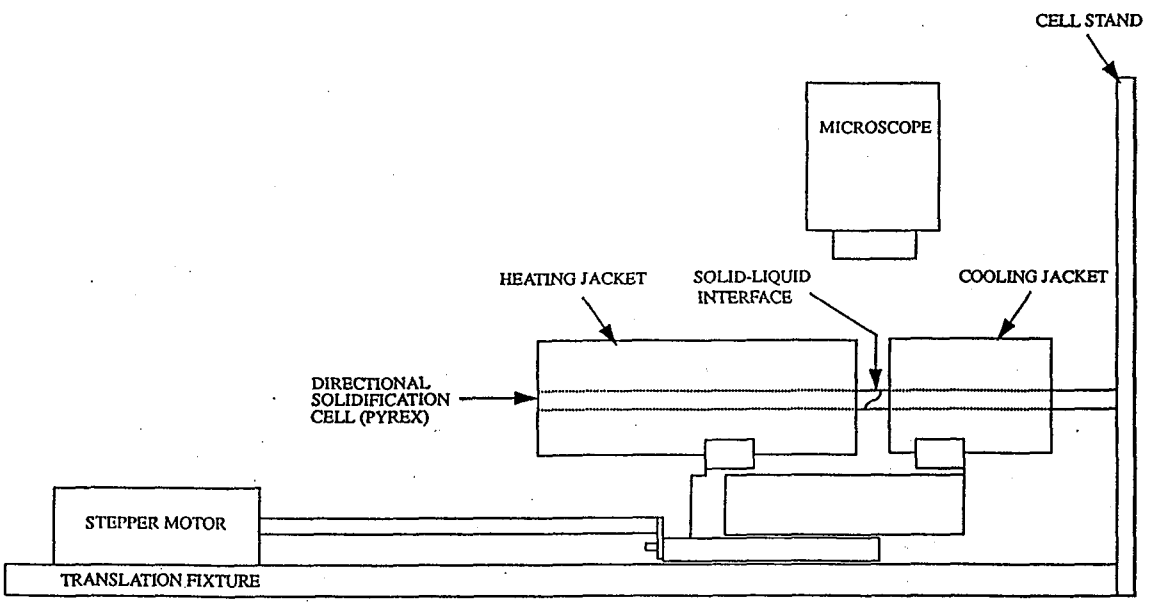

Figure 1. Schematic of the experimental apparatus, $z = 0$ is at the center of the gap.

EXPERIMENT PROCEDURE

The experiments using SCN were performed in the Low Temperature Directional Solidification Furnace (LTDSF) at the NASA Lewis Research Center; the experimental procedure has been described in detail by de Groh and Lindstrom (1994) and Yeoh (1992). A schematic of the experimental apparatus is shown in Figure 1. The LTDSF is a Bridgman type furnace employing two copper jackets, each of which has an associated constant temperature bath. The experiments were conducted with the furnace in a horizontal orientation and at furnace translation rates of 0 μm/s (for non-growth) and 40 μm/s (for steady solidification).

The heating and cooling jackets have a 1.1 cm square hole into which the ampoule fits. The borosilicate glass ampoules used have an outer square cross section of 0.775 cm and are 15 cm long with a wall thickness of approximately

0.0925 cm. The corners of the ampoule are slightly rounded as depicted in Fig. 2(a). The ampoule was filled under vacuum with SCN which was purified to eliminate solutal convection. The physical properties of SCN and of the glass ampoule have been listed elsewhere (de Groh and Lindstrom, 1994). In this paper we shall consider two experiments: the no-growth experiment (referred to as SCN-4) and the steady solidification experiment (SCN-8). (In addition to these two experiments, work by de Groh and Lindstrom (1994) also includes a steady melting experiment. Because of the limited space, this third experiment will be analyzed in a future publication).

In all experiments, the heating and cooling jackets were maintained at a temperature difference of $63°C$ with a hot zone temperature of $78°C$ for no-growth and $75°C$ during solidification. The temperature distributions on the outer surface of the ampoule were measured with type K (Chromel-Alumel) thermocouples attached to the top, bottom, front and corners of the ampoule as shown in Fig. 2(b). The temperature of the ampoule was influenced by the furnace set point, by convection and conduction in the sample, and by natural convection in the ambient air environment around the ampoule. These effects caused the temperature distribution to vary among the top surface, the vertical sides and the bottom of the ampoule.

To measure the temperature distribution, the furnace was moved relative to the ampoule in discrete steps during no growth. After each step movement of the furnace, the system was allowed to equilibrate for about 10 minutes before temperature measurements were taken. This gave the temperature distribution of the ampoule as a function of distance from the s/l interface. The temperature and position measurement accuracies are estimated to be approximately $\pm 1°C$ and ± 0.5 mm.

In the no-growth case, temperature was also measured inside the SCN sample with one thermocouple located at the center and the other between the center and the upper wall. These two thermocouples, designated in Fig. 2(b) by T_c and T_u respectively, provided temperature distributions along two longitudinal directions, i.e. the lines $(0, 0, z)$ and $(1.54mm, 0, z)$.

A microscope and camera were used to examine the s/l interface. The interface location and shape was quantitatively analyzed at the mid-center vertical plane (MCP), upper-center horizontal plane (UCP), top surface (TS) and the front surface of the SCN sample (FS). In the coordinate system shown in Fig. 2, the MCP corresponds to the $(x, 0, z)$ plane. UCP is in the yz plane at $x = 1.5$mm for SCN-4 and $x = 1.0$mm for SCN-8. TS represents the intersection between the S/L interface and the inner top wall, namely the interface shape in the plane. FS refers to the intersection between the s/l interface and the inner front ampoule wall, the interface at the $(2.95mm, y, z)$ plane. Photographs were taken of the s/l interface only when steady state conditions were reached. The photographs were then traced on an electromagnetic digitizer. The shape of the interface was obtained from the digitized data. To minimize the inconsistency of the measured temperature and interface positions caused by experimental uncertainties, a simple averaging technique was used to adjust the raw experimental data. These adjusted temperature and interface position data are listed in de Groh and Lindstrom (1994).

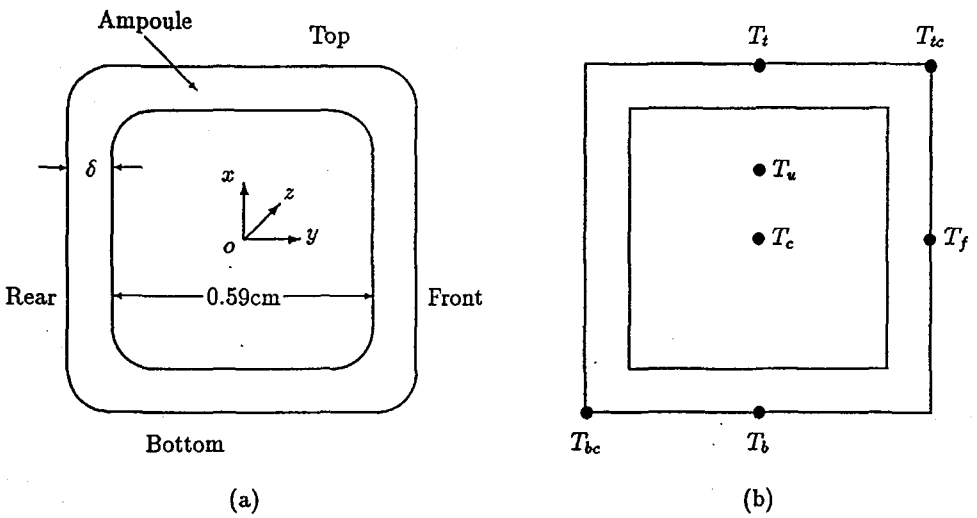

Figure 2. Schematic of the cross-section of glass ampoule and arrangements of thermocouples. (a) The rounded-corner ampoule actually used in the experiment and definition of co-ordinate system. $z = 0$ is defined as the center of the gap between hot and cold zones and the positive z-axis is directed towards the solid. $\delta = 0.0925$cm is the thickness of ampoule wall. (b) The simplified sharp-corner model used in the simulation.

The Prandtl number, $Pr = \nu/\alpha$, for SCN is approximately 23, where $\nu = 2.6 \times 10^{-6} m^2/s$ is the kinematic viscosity and α is thermal diffusivity. The thermal Grashof number is given by:

$$Gr_T \equiv \frac{g\beta_T \Delta T l_c^3}{\nu^2}$$

where $\beta_T = -8.1 \times 10^{-4}/K$, is the coefficient of thermal expansion. Since we are considering horizontal growth, $\Delta T = 18K$ is the temperature difference between the hot zone and the melting temperature, and the distance over which this gradient acts is l_c, the characteristic length of the system ($l_c = 2cm$). Under these conditions at unit gravity, $g = 9.8m/s^2$, the thermal Grashof number is about 1.7×10^5.

NUMERICAL MODELING

Governing Equations

The mathematical model used in the present work considers heat transport in both SCN and the glass ampoule, fluid motion in the melt, and phase change at the S/L interface. The liquid SCN is assumed to be Newtonian and its motion is described by the following Navier-Stokes equation:

$$\rho_0 \left(\frac{\partial \mathbf{u}}{\partial t} + \mathbf{u} \cdot \nabla \mathbf{u} \right) = -\nabla p + \nabla \cdot [\mu(\nabla \mathbf{u} + (\nabla \mathbf{u})^T)] + \rho_0 \mathbf{g}[1 - \beta_T (T - T_0)] \quad (1)$$

where $\mathbf{u}$ is the velocity vector, t is time, ρ_0 is fluid density, p is pressure, μ is viscosity, T is temperature, T_0 is a reference temperature, $\mathbf{g}$ is the acceleration of gravity, β is the volumetric expansion coefficient and the Boussinesq model is adopted to approximate the buoyancy force caused by density variation with temperature. The incompressibility condition for liquid SCN is given by

$$\nabla \cdot \mathbf{u} = 0 . \quad (2)$$

The heat transport is controlled by the balance of thermal energy

$$\rho_0 c_p \left(\frac{\partial T}{\partial t} + \mathbf{u} \cdot \nabla T \right) = \nabla \cdot (\kappa \nabla T) \quad (3)$$

where c_p is specific heat, κ is thermal conductivity. To model the borosilicate glass ampoule we treat the ampoule walls as solid and consider only the heat conduction equation (3) within the wall regions. Since the temperature levels considered were low, radiative heat transfer was neglected in this work.

The boundary conditions associated with eqn. (1) are the no-slip conditions imposed at the SCN/ampoule interface. For eqn. (3), the interpolated temperature profiles based on the experimental measurements are specified on the outer surface of the ampoule. Note that the numerical simulation incorporates conduction through the ampoule.

At the s/l interface, the following phase change conditions need to be satisfied:

$$T_s[S(t), t] = T_l[S(t), t] = T_m , \quad (4)$$

$$(\kappa_s \nabla T_s - \kappa_l \nabla T_l) \cdot \hat{\mathbf{n}} = \rho L \frac{dS}{dt} . \quad (5)$$

The subscripts, s and l, refer to the solid and liquid regions, respectively; $S(t)$ is the spatial position of the S/L interface; T_m is the melting temperature; $\hat{\mathbf{n}}$ is the unit outward normal to the interface (pointing from liquid to solid); and L is the latent heat of fusion. Since at the macroscopic level the interfaces studied are flat, we shall not consider the influence of interface curvature on melting point (Flemings, 1974) and assume solidification to occur at the equilibrium melting temperature.

The FEM Model

In the horizontal Bridgman configuration, the longitudinal axis of the furnace is perpendicular to the gravity vector as shown in Fig. 3. Since it is reasonable to assume that the heat and flow fields are symmetric with respect to the middle center plane, only half of the ampoule is modelled in the 3-D Simulation. We consider two ampoule cross-sections. One has rounded corners, which is closer to the real ampoule used in the experiment, while the other has sharp corners.

In selecting the length of the computational domain, we considered only the central 6.25 cm of the total 15 cm length of the ampoule. Beyond the region modeled, the experimental data indicated that the temperature variations are very small and should not affect the solution near the interface.

The 2-D FEM mesh was built with the 4-node bilinear element, in which the velocity and temperature were approximated by bilinear shape functions and the pressure was approximated as piecewise constant. The typical 2-D mesh used in the modelling has 954 bilinear elements and 1026 nodes.

For the 3-D FEM model, we used the 8-node linear brick element, in which the velocity and temperature are assumed to be trilinear and the pressure to be piecewise constant. The FEM meshes were generated by FIMESH, a mesh generator provided in FIDAP. A total of four 3-D meshes were created for our computation. For each of the sharp corner and rounded corner models, we had a corresponding fine mesh and a coarser mesh. The two fine meshes are shown in Fig. 4.

In this work numerical solutions were obtained using the FEM program FIDAP, a general fluid dynamics analysis package (Engleman, 1993). For steady-state problems, the discretized FEM equations can be reduced to a set of nonlinear algebraic equations in the following matrix form

$$\mathbf{K}(\mathbf{U})\mathbf{U} = \mathbf{F} \quad (6)$$

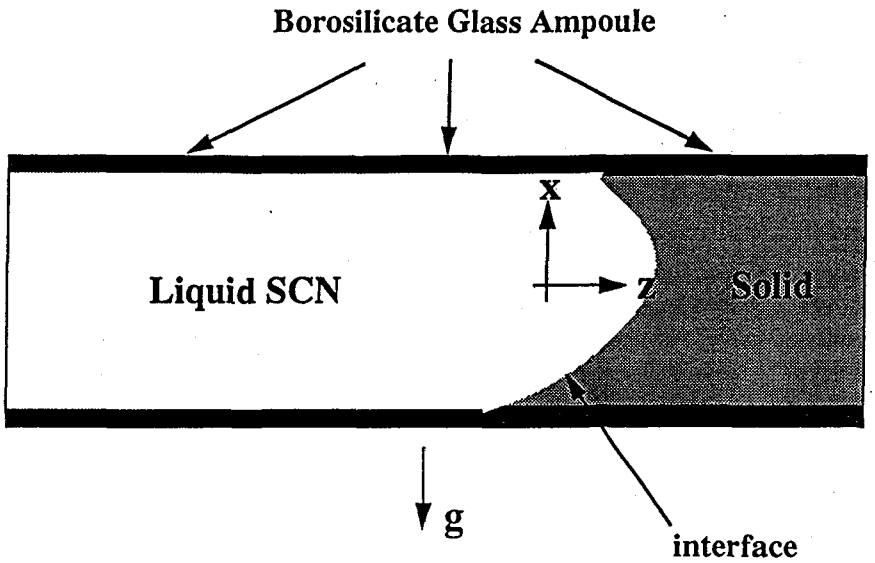

Figure 3. Schematic diagram of the simplified 2-D FEM model for the directional SCN growth experiment. For the 3-D model this diagram represents the mid-center vertical plane, i.e. the xz plane at $y = 0$.

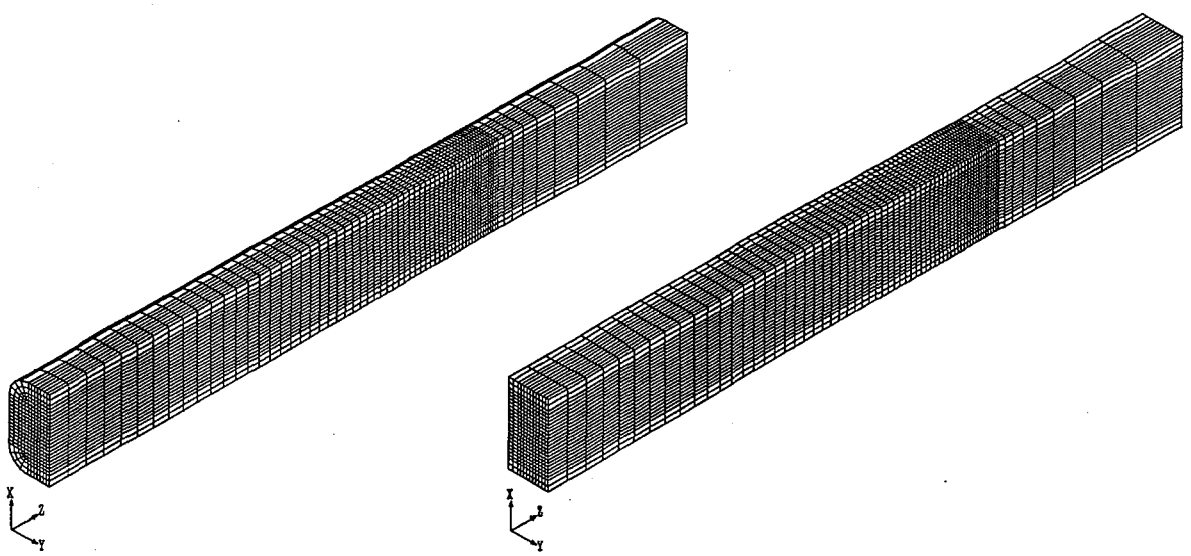

Figure 4. The two finer 3-D meshes used. On the left is the rounded corner mesh. This mesh has 18090 8-node linear brick elements with a total of 20468 nodal points. On the right is the sharp corner mesh built with 19872 elements and 22750 nodes.

where K is the global system matrix, $\mathbf{U} = (\mathbf{u}, p, T)$ is the global vector of unknowns (velocities, pressure and temperature), and F is a vector that includes the effects of body forces and gradient type boundary conditions. For the problem we considered, there is strong coupling between the momentum and the energy equations through the buoyancy term as well as through the convective terms.

The Enthalpy Method

To model the phase change in SCN, we used the enthalpy method (Crank, 1984). As a fixed domain approach, the enthalpy method avoids tracking the s/l interface by incorporating the Stefan condition (5) into the following definition of enthalpy:

$$H(T) = \int_{T_{\text{ref}}}^{T} \rho c_p(\tau) d\tau + \rho f(T) L \qquad (7)$$

where T_{ref} is an arbitrary reference temperature and f is the *local liquid volume fraction* (Crank, 1984, Voller and Swaminathan, 1990). For an isothermal phase change, f is given by the Heaviside step function

$$f(T) = \begin{cases} 0\,, & T < T_m \\ 1\,, & T > T_m \end{cases} . \qquad (8)$$

In numerical solutions, H as given in (7) usually needs to be smoothed. The following linear approximation (Yao and Chait, 1993) is used in our computation:

$$H_\varepsilon(T) \equiv \begin{cases} \rho_s c_p^s T\,, & T < T_m - \varepsilon \\ \rho_s c_p^s (T_m - \varepsilon) + & T_m - \varepsilon < T < T_m + \varepsilon \\ + \left(\dfrac{\rho_s c_p^s + \rho_l c_p^l}{2} + \dfrac{\rho_s L}{2\varepsilon} \right) [T - (T_m - \varepsilon)], & \\ \rho_s c_p^s T_m + \rho_l c_p^l (T - T_m) + \rho_s L & \\ & T > T_m + \varepsilon\,. \end{cases} \qquad (9)$$

In this approximation, the latent heat is released over a small temperature interval $[T_m - \varepsilon, T_m + \varepsilon]$, and the value of ε corresponds to the half-length of a transition zone.

Based on the definition of enthalpy an *apparent heat capacity* (AHC) can then be defined as (Crank, 1984)

$$C^A(T) \equiv \frac{\partial H}{\partial T} = \rho c_p + \rho L \delta(T - T_m) \qquad (10)$$

where δ is the Dirac function. Numerical schemes based on (10) are often referred to as the *apparent heat capacity method* (AHCM). We use the following temporal averaging scheme (Morgan et al., 1978, Dantzig, 1989) to approximate the AHC:

$$C^A \approx C_\varepsilon^A = \frac{H_\varepsilon(T^k) - H_\varepsilon(T^{k-1})}{T^k - T^{k-1}}\,, \qquad (11)$$

where k represents iteration number.

One of the difficulties inherent to the AHCM is the selection of parameter ε involved in the calculation of C_ε^A or H_ε. Detailed studies about the effect of ε value on solution accuracy and convergence with mesh refinement can be found in Shamsundar (1978), Yao and Chait (1993a), (1993b). For the AHCM with the linear approximation given in (9), numerical tests in Yao and Chait (1993a) shows that the accuracy of solutions varies with the value of ε and there exists an optimum ε at which the best accuracy may be obtained for a particular spatial and time discretization. Unfortunately, the analytical prediction of the optimum ε is not available in practice. The general rule recommended by Bonacina (1973) is to select the value of ε so that the transition zone embraces one or two complete elements. This rule was used for selecting ε values in our computations. Our study suggests that this rule produces results that are very close to the optimum ε. In enthalpy method, the s/l interface is usually recovered by computing its isotherm; its resolution is determined by the value of ε. For the no-growth case the resolution of interface is about $2\varepsilon = 0.1°C$ which is smaller than the estimated accuracy of measured temperature.

At the s/l interface or in the transition region, the fluid velocity diminishes to zero. Clearly then, the enthalpy formulation must be able to account for this velocity behavior in the vicinity of the phase-change front. There are a number of methods available in the literature (Voller, 1987). In our computation, a so-called variable viscosity method (Voller et al., 1987, Gartling, 1980) is used to model the velocity behavior. In this method, the liquid SCN is treated as a Newtonian fluid whose viscosity is a function of temperature and takes an artificially high value when T is below the melting point. This treatment has the effect of immobilizing the solid portion of the SCN so that any predicted velocities in the solid region are negligible.

Implementation of the variable viscosity method is very simple. It requires only the specification of a viscosity-temperature curve. However the artificially introduced large discontinuity in the viscosity may cause some numerical difficulties in convergence of the nonlinear iteration, especially when the segregated solution approach is used and the convection is strong (as in this work). Consequently, an incremental solution procedure is used. In this solution process, we begin with a viscosity jump across the interface of about 10^4. Then we restart from the previous solution each time with a viscosity jump increase of 10 or 10^2. Our computation stops when a viscosity discontinuity of 10^8 is reached, since our experience shows that the solution accuracy is good enough at this point.

Segregated Solution Approach

In general there are two distinct solution approaches available for solving the nonlinear system (6). The first approach solves the whole system in a simultaneous coupled manner, while the second approach solves each equation separately in a sequential segregated manner. Fully coupled solution approaches, such as successive substitution and Newton-Raphson, usually require formation of the global system matrix which includes all the unknown degrees of freedom. While this strategy is cost-effective for most 2-D problems, the peripheral storage required for 3-D problems can become excessive.

In contrast to the fully-coupled approach, the segregated solution algorithm (Haroutunian et al., 1991a and 1991b) avoids the direct formation of a global system matrix. Instead, the global matrix is decomposed into smaller sub-matrices, each governing the nodal unknowns associated with only one conservation equation. These smaller sub-matrices are then solved in a sequential manner. As the storage of the individual sub-matrices is considerably less than that needed to store the global system matrix, the storage requirements of the segregated approach are substantially less than that of the fully coupled approach. This makes it possible to solve large-scale 3-D simulation problems on a workstation. All the 3-D computations presented in this work were done on a SPARCstation†.

† SPARC is a registered trademark of SPARC international, Inc.

RESULTS AND DISCUSSION

In this section we present our numerical simulation results and compare them with experiments.

No-Growth Experiment (SCN-4)

2-D FEM Modeling

It is natural to start from a simplified 2-D model which considers the mid-center vertical plane of the ampoule (MCP) only. The measured temperature profiles given by the thermocouples T_t and T_b are imposed on the top and bottom boundaries of the 2-D model. Since the resulting global system (6) is much smaller than that in the 3-D case, the fully coupled solution approach is used for solving the nonlinear system.

The numerical results suggest that the heat and flow fields predicted by the simplified 2-D model are fairly good for the no-growth experiment. For example, the 2-D solution of temperature along the center z-axis, T_c, is very close to the 3-D solution and to experimental data, as shown in Fig. 5. The S/L interface shape of the 2-D model also compares well with the 3-D solution and the measured data, as can be seen in Fig. 6. Our results indicate that solutions of the 2-D model can provide reasonable approximations for temperature, velocity and interface shape on the symmetric planes (MCP) of the ampoule.

Visualization of 3-D Flow in the Melt

The information obtained from the 2-D model is limited to the MCP. Although the 3-D model requires much more computational effort and resources, it can provide much more detail on the interface shapes, transport phenomena and fluid flow in the whole domain. The flow pattern on the MCP indicates that the dominant flow is the so-called *shallow-cavity flow* (Arnold et al., 1991), which agrees with the experimental observation and literature. The primary characteristic of shallow-cavity flow is the single recirculating cell in the vertical (xz) planes as shown in Mennetrier et al. (1991), Yeoh (1992), and Yao and de Groh (1993). This strong convective flow cell forces hot liquid to flow along the top wall, raising and homogenizing the top wall temperature as well as directing hot liquid against the upper portion of the interface. The above mentioned fluid motion can be visualized using a trace of a particle path as shown in Fig. 7, in which a particle is released at the point $x = 0.26, y = -0.1$ & $z = -0.6$. As seen in the side view in Fig. 7(a), the liquid particle turns downward when confronted by the interface. After being cooled by the interface and the imposed thermal gradient, it returns along the bottom wall of the ampoule. The isometric perspective view in Fig. 7(b) illustrates the complex three-dimensional particle trajectory in the space between the MCP and the rear wall. Note that the spatial position of the particle in Fig. 7 is plotted at each time step. Since the time step is fixed, the distance between two particle symbols actually indicates how far the particle travels in one time step. Therefore it is clear, by examining the distance between the circular symbols on the path, that the particle flows much faster near the interface than at the other end of the domain.

Another important feature of the 3-D flow field is secondary flow in the planes perpendicular to the z-axes (i.e. the xy planes). A visualization of the secondary flows is shown in Fig. 8 in which we plot velocity vectors on different xy planes. The plot at $z = 0$ cuts the interface in the middle and captures the liquid SCN on the upper portion only. The blank lower portion in the $z = 0$ plot is the solid SCN. Moving away from the interface along the negative z-direction, a flow cell is first developed on the upper portion around $z = -0.2$cm. This flow cell grows stronger on the xy planes further away from the interface. After reaching the maximum strength, the upper cell starts decaying. Meanwhile, a second flow cell is formed in the lower part as shown by the $z = -0.4$ plot. This lower cell rotates in an opposite direction to the upper cell and is stronger in planes deeper in the hot zone. At around $z = -0.6$cm (about one seventh of the total liquid SCN length) the two counter rotating cells are about of equal strength. Then the upper cell becomes weaker and weaker, being pushed to the upper corner at $z = -3.2$ and vanishing at about $z = -3.9$. At $z = -4.1$cm, the flow is dominated by the primary flow pattern again with liquid coming along the

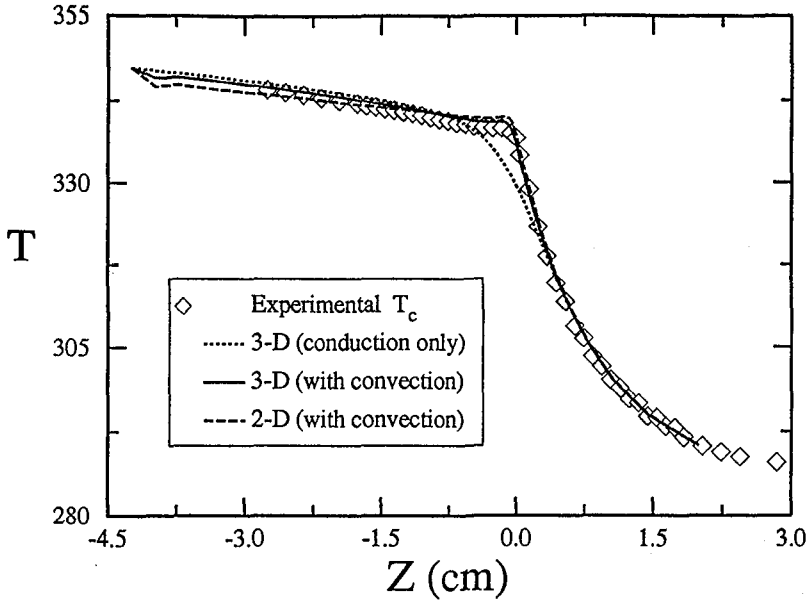

Figure 5. Comparison of 2-D and 3-D FEM solutions of temperature variation of T_c along the center z-axis, i.e. line $(x = 0, y = 0, z)$, with the experimental data.

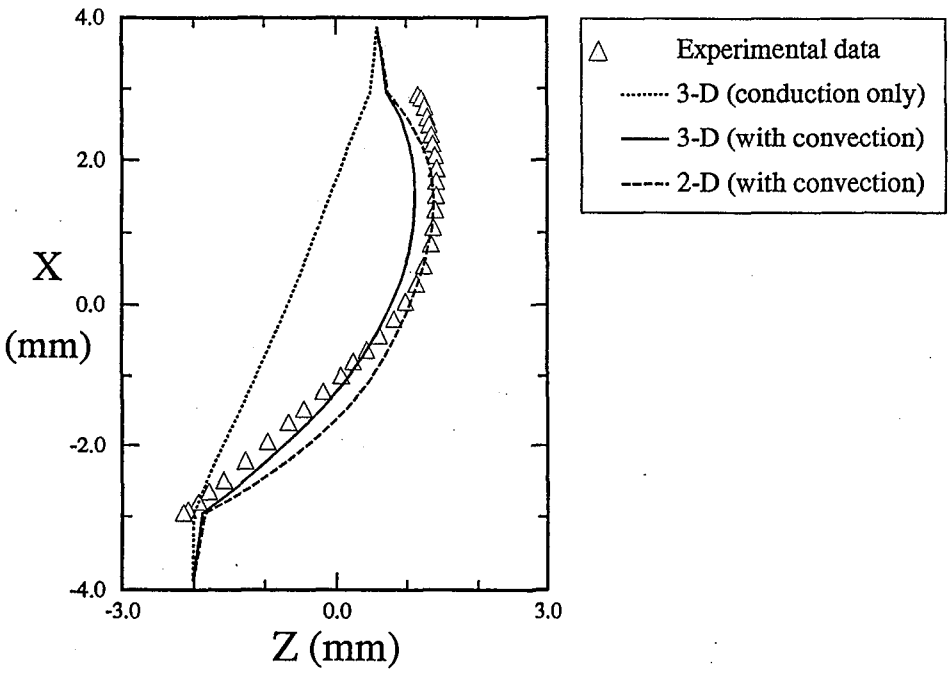

Figure 6. Simulated s/l interface shapes on the MCP based on 2-D and 3-D FEM models and comparison with the no-growth experiment (SCN-4) data.

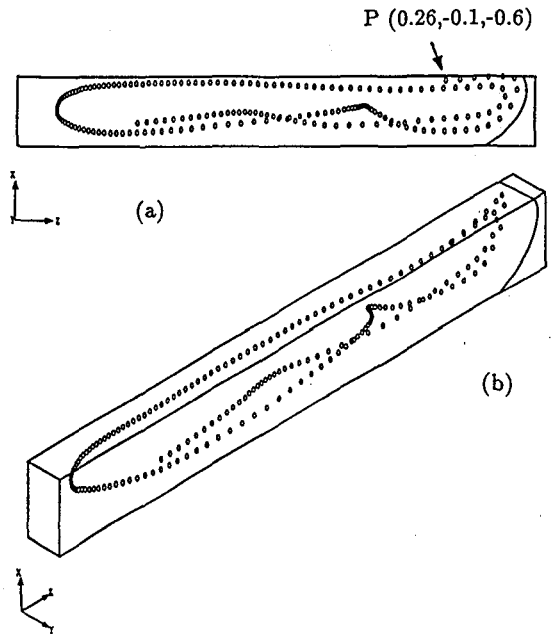

Figure 7. The particle path plotted from time 0 to 220 sec. with a fixed time step $\Delta t = 1.2$ sec for SCN-4. The particle, labelled as P, is released near the interface and MCP. (a) The side view; (b) The isometric perspective view. Note that only the liquid SCN part of the computational domain is displayed here.

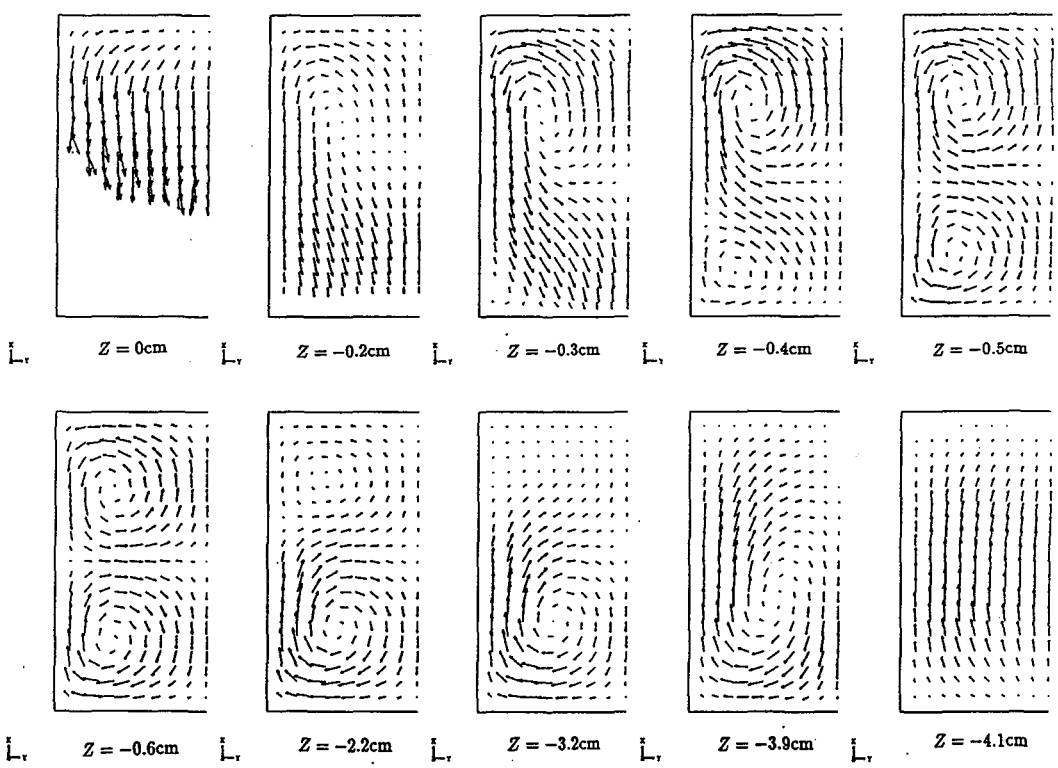

Figure 8. Visualization of the secondary flows on different xy planes for the no-growth SCN-4 experiment. The plots are based on the finer mesh for the simplified sharp corner model. Note that the plots are viewed from negative z-direction and the hot end of ampoule is $z = -4.2$cm.

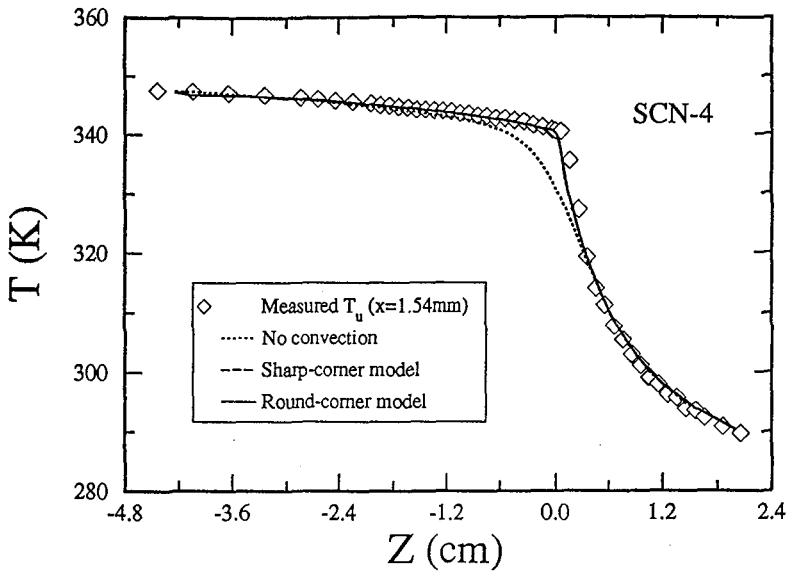

Figure 9. Computed no-growth 3-D FEM solutions of temperature variation of T_u along the upper z-axis, i.e. line $(x = 1.54mm, y = 0, z)$ using the finer round-corner and the sharp-corner meshes.

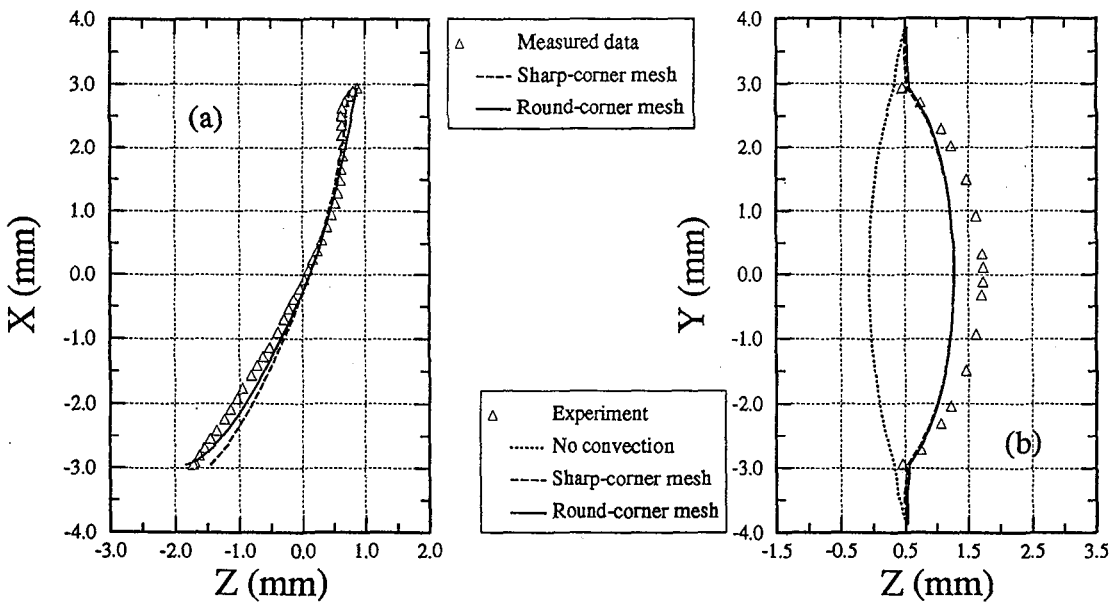

Figure 10. Modelled S/L interface shapes during no-growth solidification using the round-corner and the sharp-corner FEM meshes and comparison with the experimental measurements. (a) On the front surface of the SCN sample (FS, $y = -2.95$mm); (b) The upper center plane (UCP, $x = 1.54$mm).

bottom wall, changing direction and flowing upwards along the hot end of the ampoule, then changing direction again and flowing back along the top wall toward the interface.

Effects of Natural Convection

Our previous studies and the present work indicate that the convective flow in the melt has a great impact on the shape of s/l interface. This is shown in Fig. 6 and 12 where the interface obtained from the conduction-only solution is flat; the interface is highly curved when convection is included.

Another interesting phenomenon related to natural convection is the temperature distribution in the neighborhood of the interface. As seen in Fig. 5, the temperature variation is smooth near the interface (around $z = 0$) with a relatively wide diffusion layer when no convection is considered. However, when convection is added, there is a sharp change in the slope of the temperature curve and the diffusion layer becomes much narrower near the interface. Note the good agreement between the simulation with convection and the experimental data in Fig. 5. This narrow diffusion boundary layer and the dramatic change in slope render a great challenge to numerical modeling. We believe this phenomenon may be one of the main causes of difficulty in attaining convergence.

As noted earlier, for the cases considered, the thermal Grashof number was about 1.7×10^5 and the Prandtl number is about 23. At first, this Gr_T seems moderate, at least compared to some other horizontal systems examined by de Groh and Nelson (1994). However, SCN's relatively large Prandtl number enables larger transverse thermal gradients to develop, thus making possible the highly curved interface. Materials having a lower Prandtl number tend to result in flatter isotherms and interfaces (Gadonniex et al., 1994 and Rouzaud et al., 1993). This is reflected in the Rayleigh number, $Ra_T = Gr_T \times Pr$, which was about 4×10^6 in this study. For two other cases of horizontal plain front solidification using Bi-Sn alloys, which resulted in flatter interfaces, Rayleigh numbers were in the range of 4×10^5 (de Groh and Nelson, 1994). Thus for SCN the buoyant force/viscous force ratio is comparatively larger as compared to metals, making SCN generally more sensitive to gravity driven convection than metals.

Effects of Ampoule Corner Shape

To study the effects of ampoule shape on the thermal and flow fields, and especially the effects on the interface shapes, we examined both round-corner and simplified sharp-corner meshes as depicted in Fig. 1. The comparison between the two sets of solutions indicates that the shape of the ampoule corner has very little effect on the numerical solution. For example, on the MCP, the modelled temperature, velocity and interface shape based on the two meshes are almost identical. As a typical check, the temperature distribution of T_u on the MCP in Fig. 10 shows less than 1% difference between the solutions of T_u from the round-corner and sharp-corner meshes.

Slight differences are observed only in the vicinity of the corners. In Fig. 10(a) we compare the interface shape at the front surface of the SCN sample (FS). As shown, the interface shape given by the round-corner mesh is slightly closer to the experiment than the sharp-corner mesh solution. Another comparison of interface shape on the UCP is presented in Fig. 10(b), in which only a very small difference can be observed near the ampoule wall (at $y = \pm 2.95$mm).

Steady Solidification Experiment (SCN-8)

2-D FEM Modeling

As in the no-growth case, the 2-D model is adopted to simulate the middle center plane (MCP) of the ampoule. The measured temperature profiles of the thermocouples T_t and T_b (shown in Fig. 11) are used to specify thermal boundary conditions on the top and bottom boundary of MCP. A linear interpolation is used when the nodes fall between the raw experimental data points. To model the movement of the furnace (and hence the transient thermal environment), we assume the temperature profiles of T_t and T_b do not change with time, but translate towards the hot end with the same constant speed of 0.04mm/sec as the furnace. Since there is no direct experimental data available for an initial solution we use the steady (no-growth) analysis results as the initial condition. In our computation the Euler backward scheme with a fixed time step $\Delta t = 2$ sec is used for the time integration. The resulting global FEM system is solved by the Newton-Raphson iteration scheme.

To check the validity of the 2-D model we compare the solutions of interface location on MCP with experiment and present the results in Fig. 12. The conduction-only solution does not agree well with the experimental results and shows once again the significance of natural convection effects on the interface shape. In section 4.1 we have shown that the 2-D model provides a very good approximation for the interface shape on MCP in simulating the no-growth experiment (SCN-4). However this conclusion does not hold for modelling the solidification with non-zero growth rate. Fig. 12 shows the maximum difference between the 2-D solution (at $t = 400$sec) and the experiments to be about 3mm. This rather large difference is considered unacceptable and is much greater than the uncertainty in interface location in the experiments, which was estimated to be ± 0.5mm.

3-D FEM Simulation

The main reason for the inadequacy of the 2-D model during growth at the MCP is that the 2-D model does not have any knowledge of the 3-D effect from the rear and front ampoule walls. This does not seem to be a problem when the interface is not moving, such as the case in SCN-4 because there is less curvature in the yz plane. However when the interface moves, the 3-D effects become much more important. Our study suggests that a full 3-D model has to be used for simulating the growth of SCN-8.

Because the segregated solution approach is currently

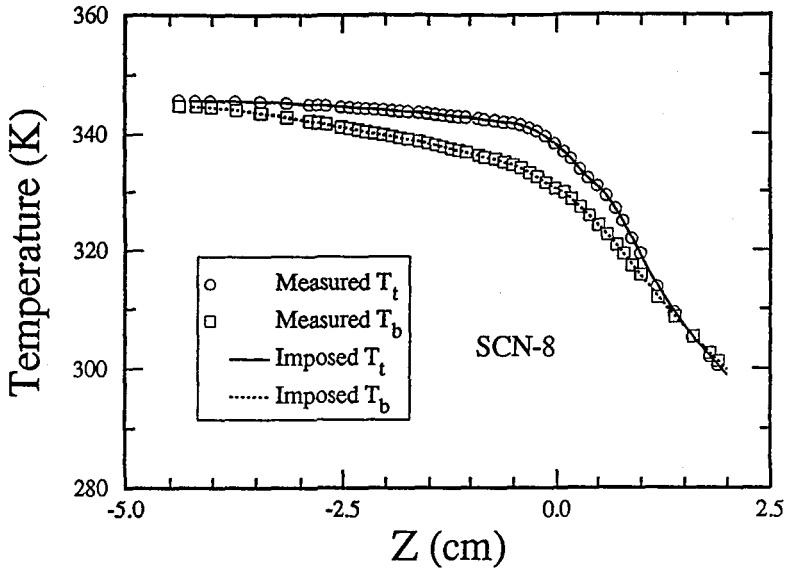

Figure 11. The measured temperature distribution of T_t and T_b along the ampoule axis. The imposed T_t and T_b are obtained by linear interpolation between experimental data points and used in the 2-D modeling as the top and bottom temperature boundary conditions. During growth the two curves are translated with a steady speed of 0.04mm/sec towards hot end.

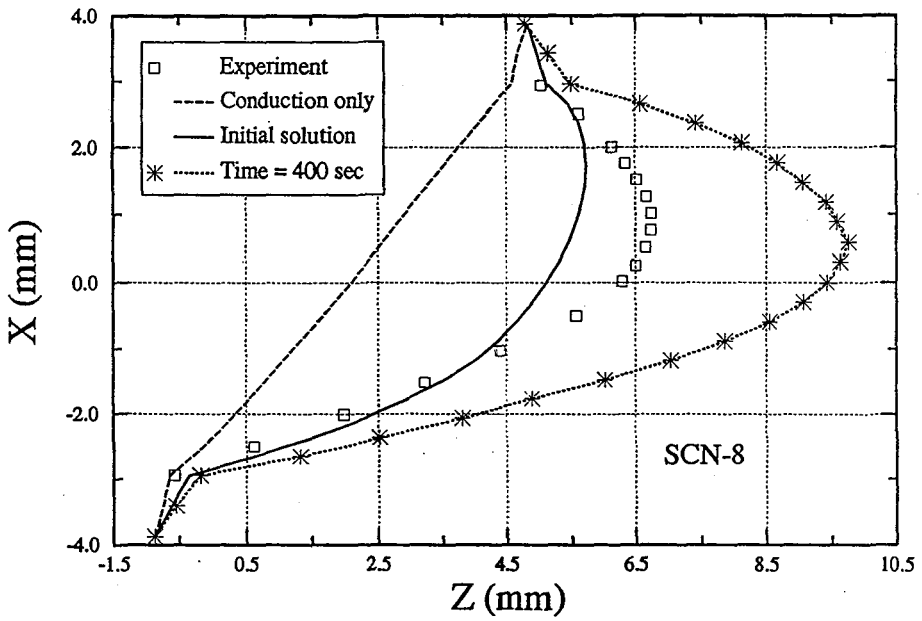

Figure 12. Simulated S/L interface shapes on the middle center plane (MCP) based on the 2-D FEM model and comparison with the experiment. The conduction-only solution is based on steady analysis with no convection. The initial solution is obtained by steady analysis considering both conduction and convection but no growth. The transient solution considers conduction, convection and a steady translation of the furnace (steady growth).

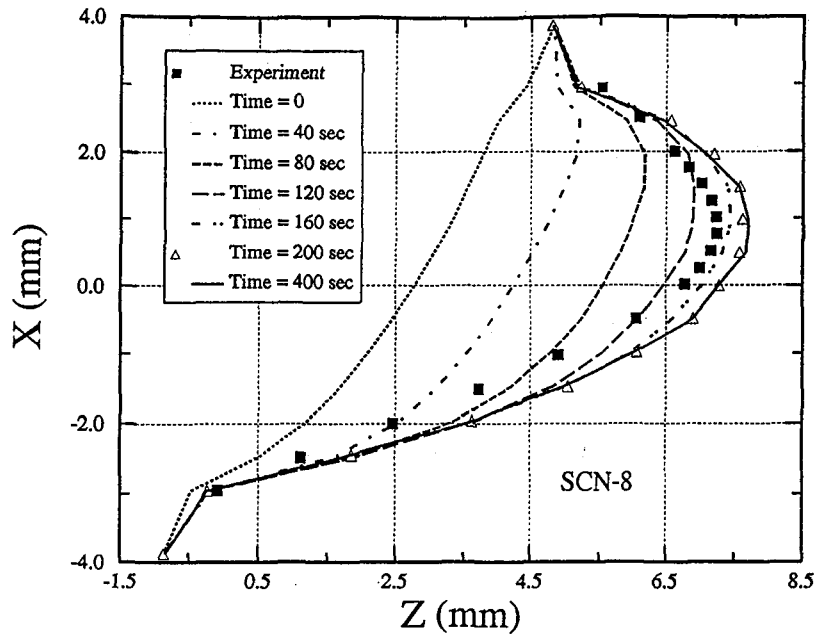

Figure 13. Development of S/L interface shapes on the MCP given by the transient 3-D FEM solidification analysis and comparison with experiment during horizontal solidification.

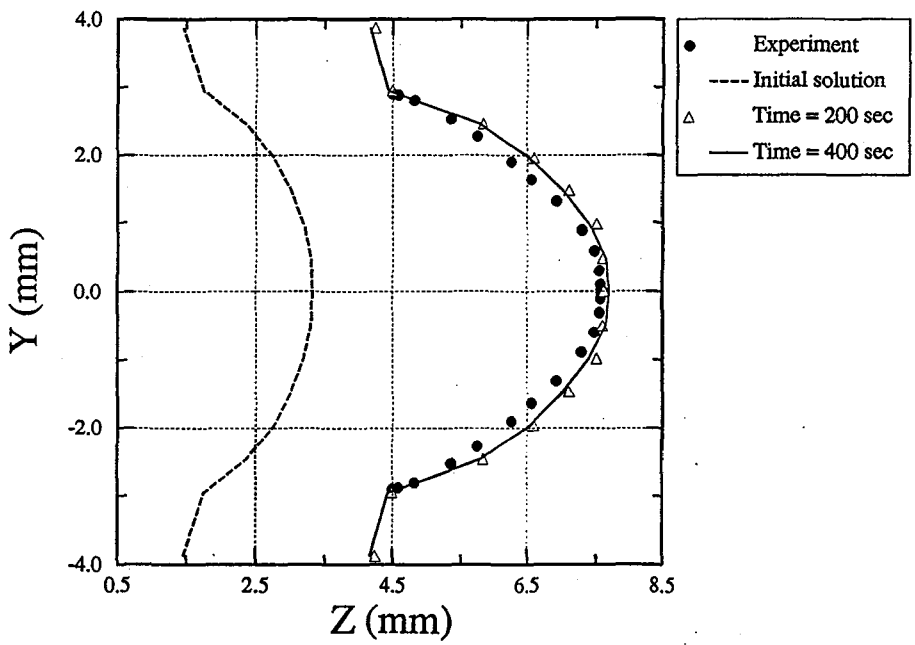

Figure 14. Simulated S/L interface shapes during solidification on the upper center plane (UCP, $x \approx 1.0$mm) and comparison with experiment.

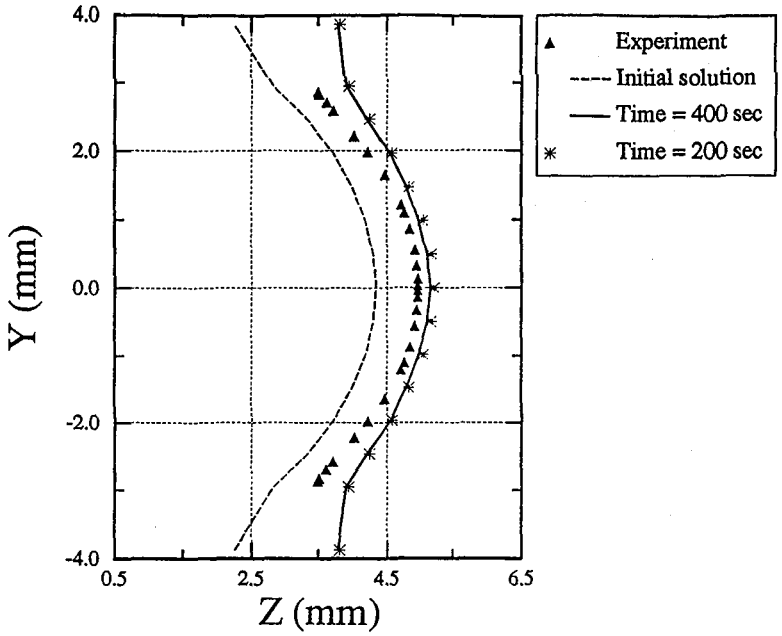

Figure 15. Computed interface shapes on the top surface of the SCN sample (TS, $x = 2.95$mm) based on 3-D transient analysis for SCN-8 and comparison with experiment.

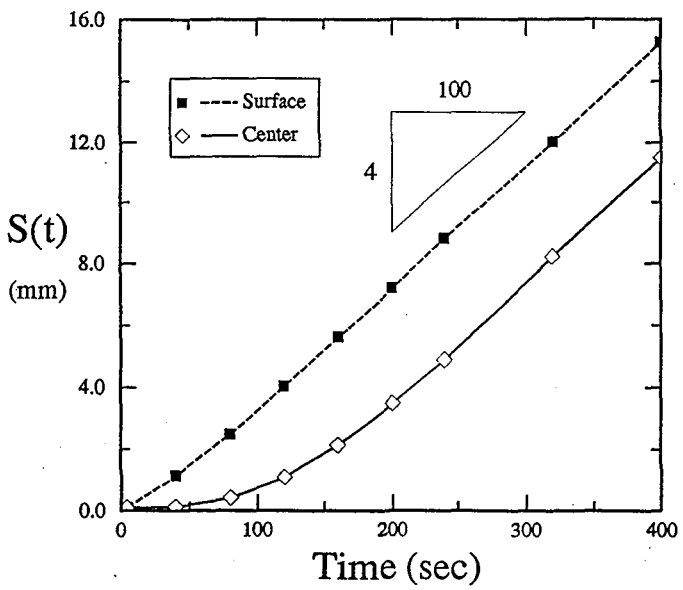

Figure 16. Time history of the interface position at the center of top surface ($x = 2.95, y = 0$) and the center ($x = 0, y = 0$) of SCN sample. The speed of the moving interface is given by the slope of the curves.

not available for transient analysis in FIDAP, the 3-D results presented in this section were obtained using the fully coupled solution approach and based on the coarse 3-D mesh with the simplified sharp corners.

The numerical evolution of the interface shape at the MCP is shown in Fig. 13. Our results indicate that the solution becomes steady after about 200 seconds. The interface shapes at $t = 200$ and 400 sec are quite close to the measured data (Fig. 13). The simulated interface shapes on the UCP and TS planes are presented in Fig. 14 and 15, respectively. The agreement between the 3-D numerical solution and the experiment is excellent.

The time history of two interface positions are shown in Fig. 16. One is at the top surface of SCN sample, i.e. along the line ($x = 2.95$mm, $y = 0$, z) and shown by the curve referred to as "surface" in Fig. 16. The other is at the center of the SCN sample. The slope of the two $S(t)$ curves represents the simulated growth rate, and the vertical distance between these two curves indicates the interface deflection between the top surface and the center. As we can see from Fig. 16, the interface shape is fully developed and the movement of the interface becomes steady when $t > 200$sec. The predicted growth rate, which is 0.04 mm/sec, is equal to the furnace translation speed used in the experiment.

CONCLUSIONS

Perhaps the most obvious advantage of using SCN for crystal growth research is its transparency, which allows quantitative determination of the s/l interface shape and simultaneous observation of important transport phenomena. The numerical and experimental investigation presented in this paper provides two complete benchmark tests for the horizontal Bridgman growth of SCN under terrestrial conditions. The excellent agreement between the numerical results and experimental measurements not only serves as a validation of the numerical model but also demonstrates the importance of the collaboration between numerical modeling and experiment.

For the two cases examined, shallow-cavity convective flow is confirmed, by our numerical and experimental observation, to be the primary flow pattern. This convective flow and its dominance in heat transfer have a significant impact on the shape of the s/l interface. As viewed from the liquid side, the s/l interface in both cases is concave in the upper half of the ampoule. This is due to the above-mentioned convecting flow which brings relatively warm liquid from the hot zone and rams it against the upper part of the interface. This flow of warm liquid moving toward the interface along the top ampoule wall with cooler liquid returning along the bottom wall, results in a dominating thermal gradient in the x-direction (with the top hotter) and interface asymmetry as viewed in the vertical (xz) planes. During solidification, as the longitudinal thermal gradient is translated along the ampoule in the negative z-direction, the liquid SCN gets cooled immediately near the ampoule wall and the s/l interface in contact with the ampoule moves with the same translation speed. However, the inner regions of the sample must conduct the heat through the poorly conducting SCN, causing solidification near the ampoule center to lag behind the outer edges. This results in a much more deflected (curved) interface for the solidification case. In addition to the effect on interface shape, natural convection in the melt has also a significant effect on the temperature distribution near the interface. Our experimental and numerical results indicate that the convection causes a very sharp thermal gradient in the liquid near the interface.

Another interesting aspect of the complex 3-D flow motion in the melt is the occurence of secondary flows in the planes perpendicular to the ampoule axes. The flow visualization based on our numerical simulation shows a complex flow structure with multiple flow cells in the xy planes which vary along the ampoule axes. The typical pattern of the secondary flow consists of two counter rotating flow cells on each side of the mid-center vertical (symmetric) plane (MCP). The upper flow cell flows down along the vertical rear (and front) wall and up at the MCP. The lower flow cell brings the fluid up along the vertical ampoule walls and down at the MCP.

In the no-growth case, the 2-D model provides a good approximation for the interface shape and the primary flow pattern on the MCP. However, for non-zero growth rate, the 2-D model is not adequate and 3-D modeling must be used. Comparisons between the two sets of solutions obtained from the round-corner and the simplified sharp-corner meshes also suggest that the shape of the ampoule corner does not have a significant effect on the numerical solution.

Our experimental examination is continuing with 3-D fluid flow velocity measurements in the SCN liquid near the interface. The valuable experience gained from our comparisons between experiments and simulations, and the good agreement achieved thus far, enables us to more confidently apply the code to other modelling cases (Yao et al., 1993, Yao and de Groh, 1994).

ACKNOWLEDGMENTS

This work was supported by NASA's Microgravity Science and Application Program (grant code # NCC 3-208). Thanks are due T. Lindstrom for extensive assistance with the SCN solidification experiments. The authors also thank T. Glasgow, E. Nelson from NASA Lewis Research Center and the other two anonymous reviewers for their comments and corrections on the manuscript.

REFERENCES

Arnold, W.A., Jacqmin, D.A., Gaug R.L. and Chait, A., 1991, "Three-Dimensional Flow Transport Modes in Directional Solidification During Space Processing," J. Spacecraft Rockets , vol. 28, pp. 238-243.

Brown,R.A., 1988, "Theory of Transport Process in Single Crystal Growth from the Melt," AIChE J., Vol. 34 (6), pp. 881-911.

Chait, A., 1990, "Transport Phenomena in Space Processing: A Modelling Approach," presented at the XX ICHMT Int'l Symposium on Manufacturing and Materials Processing , Dubrovnik, Yugoslavia,.

Chang, C.J. and Brown, R.A., 1984, "Natural Convection in Steady Solidification: Finite Element Analysis of a Two-Phase Rayleigh-Benard Problem," J. Comp. Phys., vol. 53 pp. 1-27.

Chopra, M.A. and Glicksman, M.E., 1988, "Measurement of the Diffusion Coefficient of Acetone in Succinonitrile at Its Melting Point," J. Crystal Growth , vol. 90, pp. 543-546.

Chopra, M.A., Glicksman, M.E. and Singh, N.B., 1988, Met. Trans. A , vol. 19A, pp. 3087-30xx.

Crank, J., 1984, Free and Moving Boundary Problems, Clarendon Press, Oxford, chapters 3 and 6.

Dantzig, J.A., 1989, "Modeling Liquid-Solid Phase Changes with Melt Convection, Int. J. Num. Meth. Eng. , Vol. 28, 1769-85.

de Groh III, H.C. and Lindstrom, T., 1994, "Interface Shape and Convection during Solidification and Melting of Succinonitrile, NASA Tech. Memorandum 107724, NASA Lewis Research Center, (in press).

de Groh III, H.C. and Nelson, E.S., 1994, "On Residual Acceleration During Space Experiments," submitted to the 1994 ASME Winter Annual Meeting, Chicago IL, Nov. 13-18.

Engleman, M., 1993, FIDAP Theoretical Manual (version 7), Fluid Dynamics International, Inc., 500 Davis St. Suite 600, Evanston, IL 60201.

Flemings, M.C., 1974, Solidification Processing, McGraw-Hill, p. 95.

Gartling, D.K., 1980, "Finite element analysis of convective heat transfer problems with change of phase," in Computer Methods in Fluids, Morgan, K. et al. (eds), Pentech, London, pp. 257-284.

Gadonniex, D., Gokhale, A. and Abbaschian, R. 1994, "Morphological Stability of Faceted Solid/ Liquid Interfaces in Dilute Bi-Sn Alloys," 32nd Aerospace Sci. Meeting, AIAA 94-0791.

Glicksman, M.E., Coriell, S.R. and McFadden, G.B., 1986, "Interaction of Flows with the Crystal-Melt Interface," Ann. Rev. Fluid Mech. , vol. 18, 307-335.

Haroutunian, V., Engelman, M. and Hasbani, I., 1991a, "Segregated Finite Element Algorithms for the Numerical Solution of Large-Scale Incompressible Flow Problems," presented at the Fourth International Symposium on Computational Fluid Dynamics, Davis, California, September; also submitted to Inter. J. Num. Methods in Fluids.

Haroutunian, V. M. Engelman and I. Hasbani, 1991b, "Three Segregated Finite Element Solution Algorithms for the Numerical Solution of Incompressible Flow Problems, Proceedings of the Sixth International Conference in Australia on Finite Element Methods, Sydney, Australia, July, vol. 1, G.P. Steven, C. McIvor and D.W. Kelly (eds.), University of Sydney, Australia, pp. K102-K122, .

Inotomi, Y., Miyashita, H. et. al., 1993, "Influence of Mixing in Liquid on Unidirectional Solidification Rate in Transparent Organic Alloy," J. Crystal Growth , vol. 130, pp. 85-95.

Langlois, W.E., 1985, "Buoyancy-Driven Flows in Crystal Growth Melts," Ann. Rev. Fluid Mech., vol. 17, pp. 191-215.

Mennetrier, C., Chopra, M.A. and de Groh III, H.C., 1991, "Effect of Thermal Convection on the Shape of a Solid-Liquid Interface," FED-vol. 111, Forum on Microgravity Flows, ASME , pp. 5-10.

Mogan, K., Lewis R.W. and Zienkiewicz, OZ., 1978, "An Improved Algorithm for Heat Conduction Problem with Phase Change," Int'l J. Num. Methods Eng., Vol. 12, pp. 1191-1195.

Pimputkar, S.M. and Ostrach, S., 1981, "Convective Effects in Crystals Grown from Melt," J. Crystal Growth , vol. 55, pp. 614-646.

Rouzaud. A., Comera, J., Contamin, C., and J.J. Favier, 1993, "Ground Results of the MEPHISTO Program: Benefits and Space Experiments Orientation," Microgravity sci. technol. VI/2, pp. 84- 87.

Shamsundar, N., 1978, "Comparison of Numerical Methods for Diffusion Problems with Moving Boundaries", in Moving Boundary Problems, Wilson D.G. and Boggs, P.T. (eds), Academic Press, New York, pp. 165-185.

Sparrow, E.M., Ramsey, J.W. and Harris, S., 1979, "Freezing Controlled by Natural Convection," J. Heat Transfer , vol. 101, pp. 578-584.

Voller, V.R. and Swaminathan, C.R., 1990, "Fixed Grid Techniques for Phase Change Problems: A Review," Int'l J. Numer. Methods Eng., Vol. 30, pp. 875-898.

Voller, V.R., Cross, M. and Markatos, N.C., 1987, "An Enthalpy Method for Convection/Diffusion Phase Change," Int'l J. Num. Methods Eng., Vol. 24, pp. 271-284.

Yao, M. and de Groh III, H.C., 1993, "A Three-Dimensional

Finite Element Method Simulation of Bridgman Crystal Growth and Comparison with Experiments," Num. Heat Transfer, Part A: Applications , vol. 24, pp. 393-412.

Yao, M. and Chait, A., 1993a, "An Alternative Formulation of the Apparent Heat Capacity Method for Phase Change Problems," Num. Heat Transfer, Part B: Fundamentals , vol. 24, pp. 279-300.

Yao, M. and Chait, A., 1993b, "Application of the Homographic Approximation in the Enthalpy Method for Phase Change Problems," Int. J. Num. Methods Heat & Fluid Flow, vol. 3, pp. 157-172.

Yao, M., Matthiesen, D.H. and Chait, A., 1993, "A Numerical Simulation of Heat and Mass Transport in the GTE GaAs Experiment," Proceedings of the 5th FIDAP Users Conference, May 2-4, Chicago, Illinois.

Yao, M. and de Groh III, H.C., 1994 "Numerical Modelling of Bridgman Growth in Space with MEPHISTO, prepared for 1994 ASME Winter Annual Meeting.

Yeoh, G.H., Behnia, M., de Vahl Davis, G. and Leonardi, E., 1990, "A Numerical Study of Three-Dimensional Natural Convection During Freezing of Water," Int'l J. Num. Meth. Eng. , vol. 30, pp. 899-914.

Yeoh,G.H., de Vahl Davis, G., Leonardi, E., de Groh III, H.C. and Yao, M., 1992, "A Numerical and Experimental Study of Natural Convection and Interface Shape in Crystal Growth," 1st International Conference on Transport Phenomena in Processing, PIThE, Hawaii.

Yeoh, G.H., 1992, "Natural Convection in A Solidifying Liquid," Chapter 7, Ph.D. Thesis, University of New South Wales, Australia.